Supporting Information

Heteroatom Doping-Induced Defected Co_3O_4 Electrode for High-Performance Lithium Oxygen Battery

Peng Zhang, Zhongxiao Wang, Peng Wang, Xiaobin Hui, Danyang Zhao, Zhiwei Zhang* and Longwei Yin*

Key Laboratory for Liquid-Solid Structural Evolution and Processing of Materials, Ministry of Education, School of Materials Science and Engineering, Shandong University, Jinan 250061, P. R. China

Corresponding Authors:

Email: zhangzhiwei@sdu.edu.cn;

Email: yinlw@sdu.edu.cn. Tel.: + 86 531 88396970. Fax: + 86 531 88396970 (L. Yin).

Experimental section

Materials synthesis

Synthesis of Co_3O_4

The typical synthetic procedure of Co_3O_4 was modified on the basis of the previous report.[1-2] Firstly, 0.036 mol cobalt nitrate hexahydrate ($Co(NO_3)_2·6H_2O$) and 0.009 mol sodium hydroxide (NaOH) were dissolved in 30 ml and 5 ml of deionized water, respectively. After stirring for 0.5 h, NaOH solution was added into $Co(NO_3)_2$ solution dropwise and the mixed solution went on stirring for another 0.5 h, following by transferring into a 50 mL Teflon-lined autoclave. The hydrothermal process was conducted at 180 ℃ for 6h. The obtained products were cleaned with ethanol and deionized water for several times, subsequently dried in a vacuum oven for 12 h at 80 ℃.

Synthesis of S-Co_3O_4 and P-Co_3O_4

P-Co_3O_4 was fabricated through low-temperature phosphorization method, using sodium hypophosphite ($NaH_2PO_2·H_2O$) as phosphorus source. Concretely, the obtained Co_3O_4 product (50 mg) and $NaH_2PO_2·H_2O$ (80 mg) were placed at two separated quartz boat with $NaH_2PO_2·H_2O$ at the upstream side in a tube furnace. The samples were heated at 300 °C for 2 h with a ramp of 2 °C/min under slow argon gas flow, and cooled down naturally to room temperature. To prepare S-Co_3O_4, S powder (60 mg) was used as S source via the same heating procedure. In order to avoid the influence of annealing, pure Co_3O_4 sample was also heated at the same way without any $NaH_2PO_2·H_2O$ and S powder.

Materials Characterization

The morphology of samples and discharge product were identified by SU-70 field emission scanning electron microscope (FE-SEM-70) and high resolution transmission electron microscopy (HRTEM, JEM-2100 at an acceleration voltage of 200 kV) equipped with energy dispersive spectrometry (EDS). The sample for HRTEM was cut on Leica Ultracut UCT ultramicrotome (UC7) to reduce the thickness. The phase structure and chemical components were characterized by X-ray diffraction (XRD, Rigaku D/Max-KA diffractometer using Cu Kα radiation (λ=1.5406 Å)), X-ray photoelectron spectroscopy (XPS, ESCALAB 250 spectra with 150 W Al Kα probe beam), Raman spectroscopy (JY HR800), ICP Optical emission spectrometer Varian 720-ES (ICP-ES) and Fourier transform infrared spectroscopy (FTIR, Bruker Vector 22 system). The electron spin resonance (ESR) spectra were recorded using a Bruker EMX spectrometer (X band) at room temperature.

Electrochemical Measurements

The electrochemical performances of Co_3O_4, S-Co_3O_4 and P-Co_3O_4 were evaluated using 2032 coin-type cells with gas holes. The electrode was prepared by dissolving each of the as-prepared sample (50 wt%), carbon black (40 wt%) and polyvinylidene fluoride (PVDF, 10 wt%) in N-Methyl pyrrolidone (NMP) and dip-coating the obtained slurry on carbon paper. After drying at 80 °C for 24 h, the as-prepared electrode was assembled with Li metal anode, glass fiber separator (Whatman, GF/D) and organic electrolyte (1 M LiTFSI/TEGDME) in an argon-filled glove box (H_2O< 0.5 ppm, O_2< 0.5 ppm). The mass loading of cathode is about 1 mg cm^{-2}. All of the electrochemical measurements were carried out under a 1.0-bar dry oxygen atmosphere (> 99.999%) at room temperature. Galvanostatic discharge profiles were measured on LAND CT2001A battery system (Wuhan, China) within the voltage window of 2.0-4.5 V. Cyclic voltammetry (CV, within the voltage window of 2.0-4.5 V at 0.1 mV s^{-1} speed) and electrochemical impedance spectroscopy (EIS, in a frequency range of 0.01–10^5 Hz.) analysis were performed on an electrochemical workstation (PARSTAT2273).

Computational Details

The Vo formation energy and LiO_2 adsorption energy on (100) plane of each samples were investigated using the Vienna ab initio simulation packages (VASP) with the projector augmented wave (PAW) method.[3-4] The exchange-correlation energy was described by the generalized gradient approximation Perdew-Burke-Ernzerhof (GGA-PBE). The simulated surfaces were separated by a vacuum slab of 15 Å in c-axis to avoid the interactions between the periodically repeated images. The plane wave kinetic energy cutoff and the convergence criterion were set to 420 eV and 1×10^{-6} eV, respectively. The Brillouin zone was sampled by a 3 × 3 × 3 k-point mesh for crystals and slabs calculations. The atomic geometries were relaxed until Hellmann–Feynman forces on each atom are reduced to less than 0.05 eV $Å^{-1}$ during structure optimization. The adsorption energy (ΔE_{ads}) was denoted as: $\Delta E_{ads} = E_{sub+LiO_2} - E_{sub} - E_{LiO_2}$, where $E_{sub+LiO_2}$ stands for the sum energy of the optimized substrate/LiO_2 system, E_{sub} and E_{LiO_2} are on behalf of the total energies of the bare substrate and isolated LiO_2, respectively.

Supporting Figures and Tables

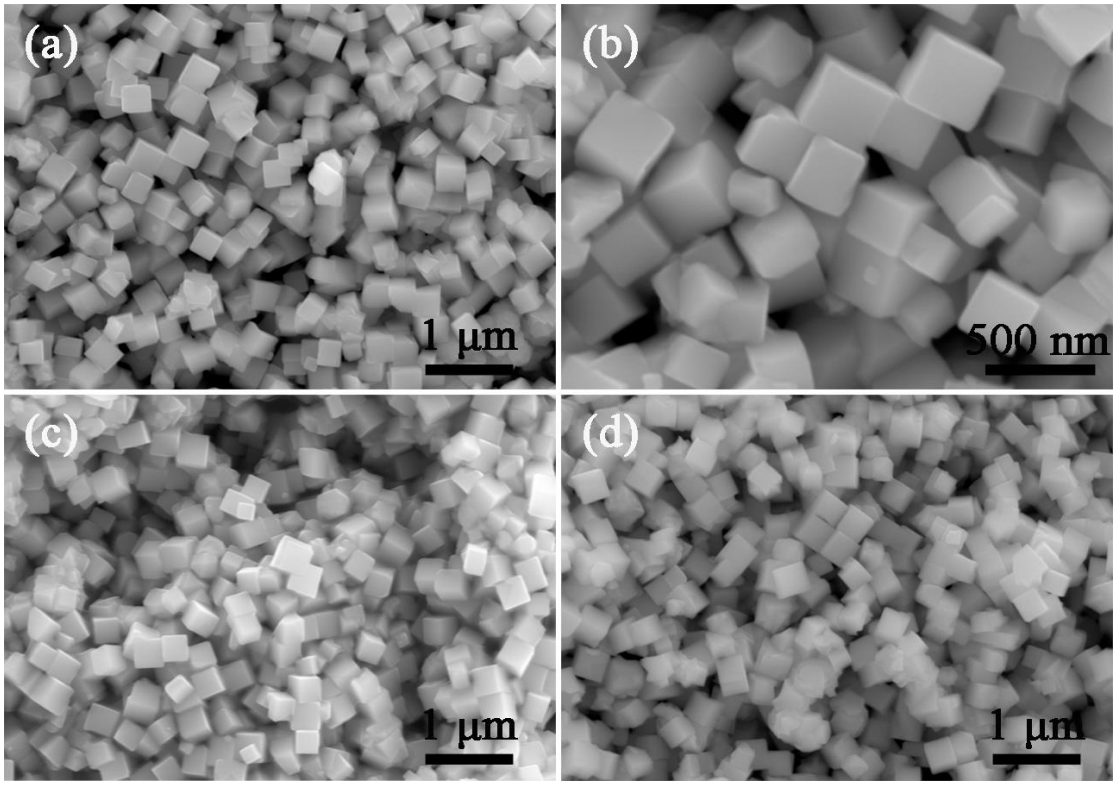

Figure S1. SEM images of (a, b) Co_3O_4 (c) S-Co_3O_4 and (d) P-Co_3O_4.

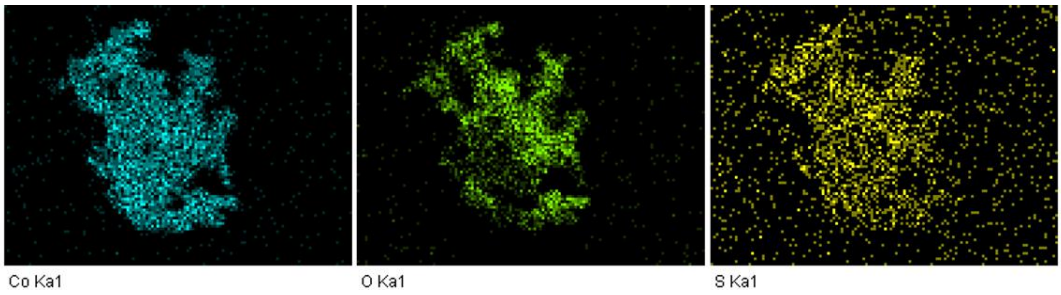

Figure S2. EDS mapping of S-Co_3O_4.

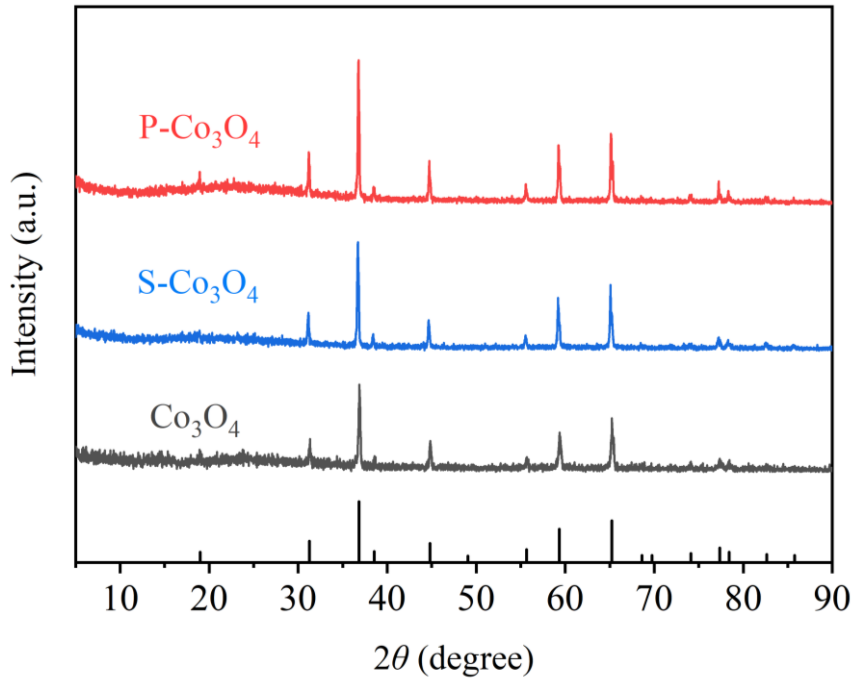

Figure S3. XRD patterns of Co_3O_4, S-Co_3O_4 and P-Co_3O_4.

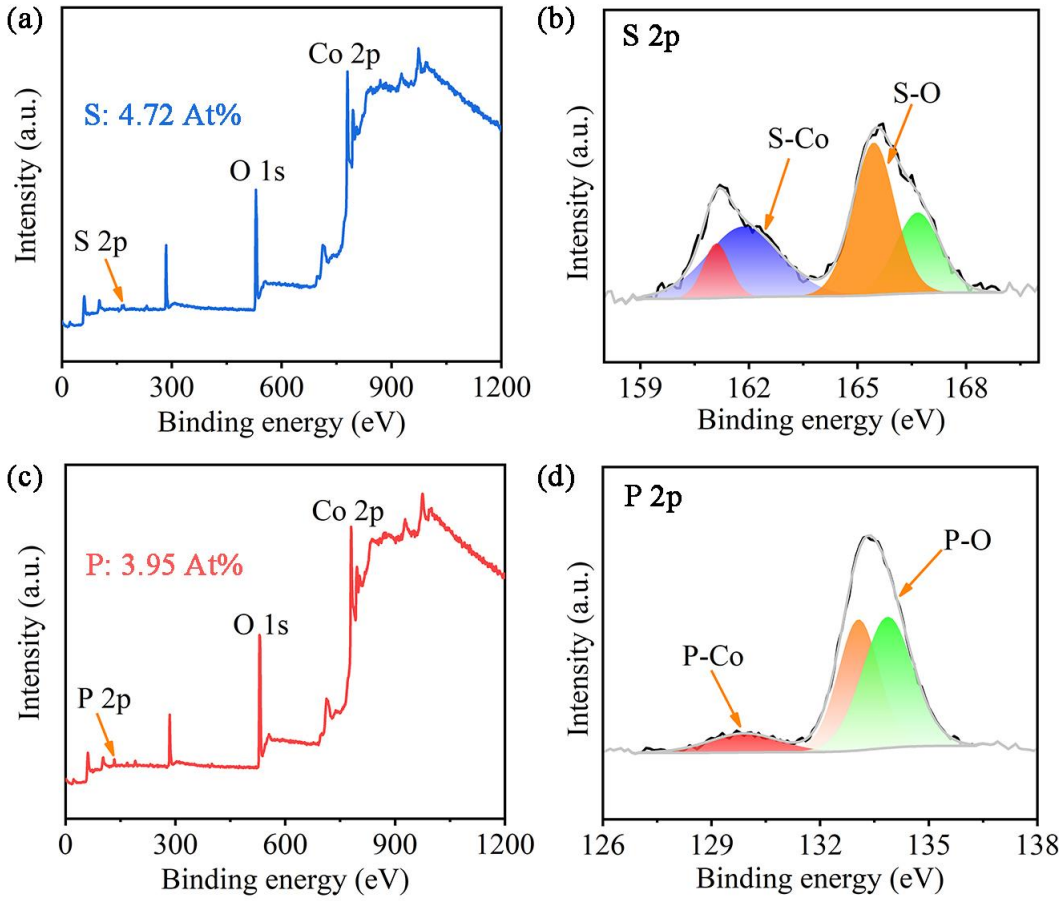

Figure S4. (a) XPS survey spectrum and (b) High-resolution XPS S 2p spectra of S-Co_3O_4. (c) XPS survey spectrum and (d) High-resolution XPS P 2p spectra of P-Co_3O_4.

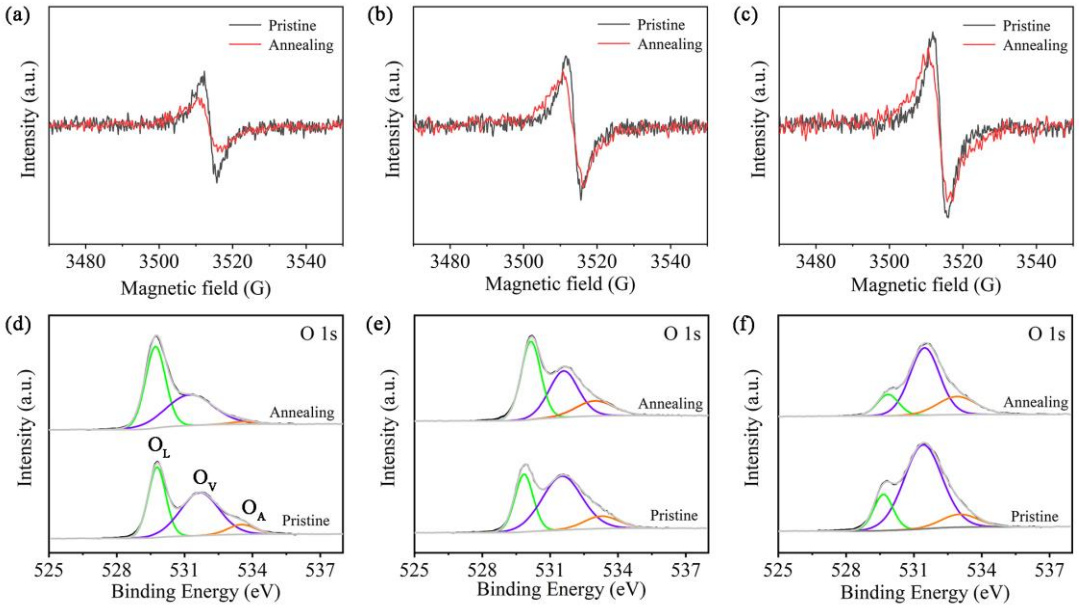

Figure S5. The characterization of stability of Vo for three samples. EPR spectra of (a) Co_3O_4, (b) S-Co_3O_4 and (c) P-Co_3O_4 before and after annealing in air. High-resolution XPS O 1s spectra of (a) Co_3O_4, (b) S-Co_3O_4 and (c) P-Co_3O_4 before and after annealing in air.

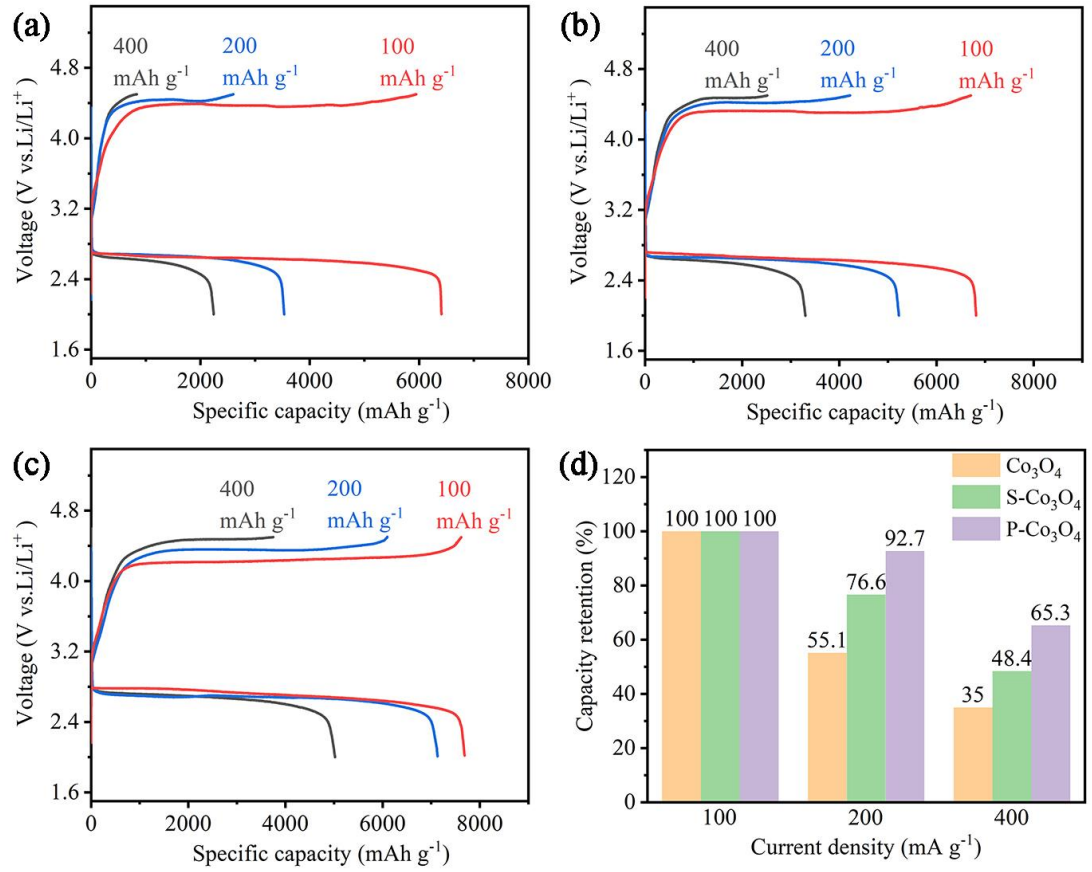

Figure S6. Discharge-charge curves at different current densities. (a) Co_3O_4. (b) S-Co_3O_4. (c) P-Co_3O_4. (d) The capacity retention of the three kinds of electrodes.

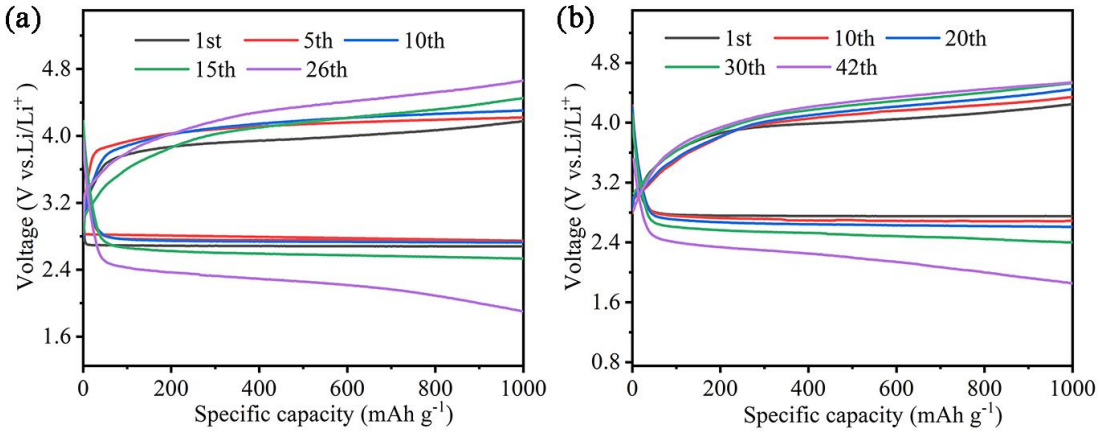

Figure S7. Discharge-charge profiles with different cycles at 100 mA g^{-1}. (a) Co_3O_4. (b) S-Co_3O_4.

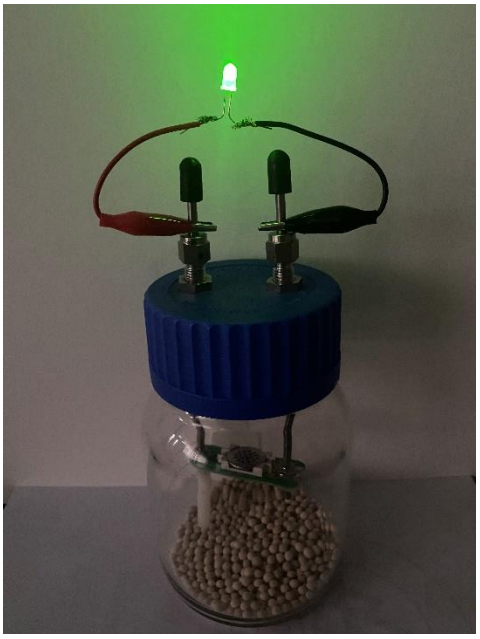

Figure S8. Photo image of the green LED powered by P-Co_3O_4-based Li-O_2 battery.

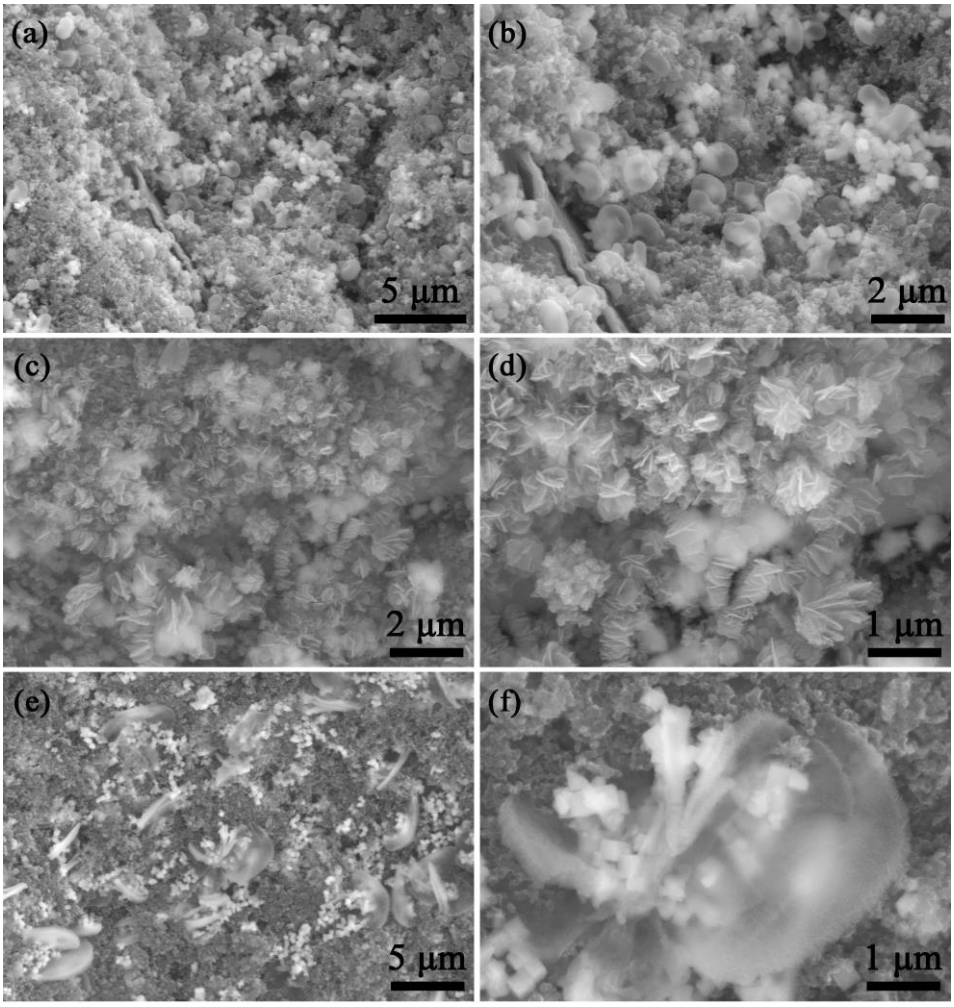

Figure S9. SEM images of three electrodes after fully discharged with different magnitude. (a, b) Co_3O_4. (c, d) S-Co_3O_4. (e, f) P-Co_3O_4.

Comments: The order of Figure S9 c/d and e/f is reverse. Therefore, we exchanged the the order of Figure S9 c/d and e/f. We confirm that the deletion will not do harm to the integrality and veracity of this work.

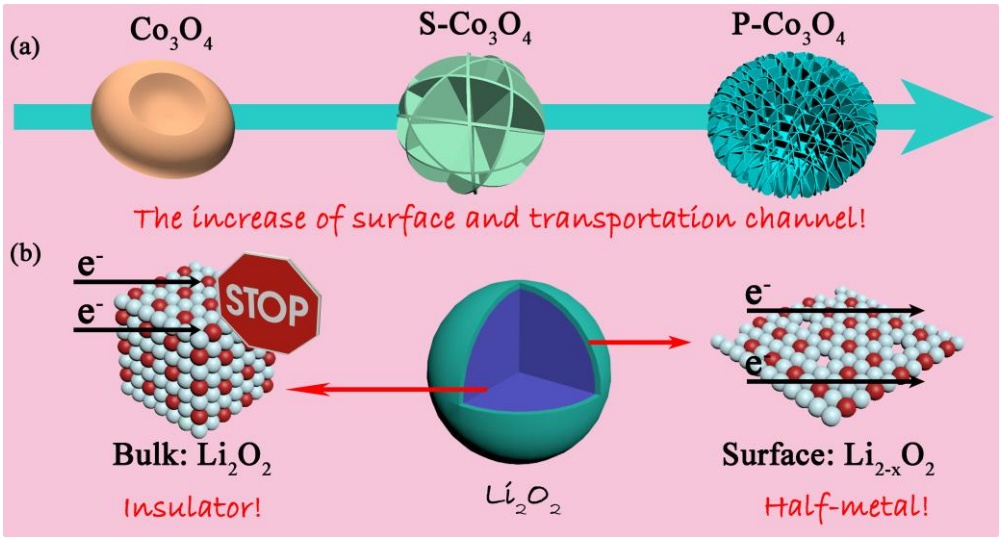

Figure S10. (a) The morphology changes of Li_2O_2 for Co_3O_4, S-Co_3O_4 and P-Co_3O_4. (b) Schematic illustration of electronic conductivity for Li_2O_2 surface and inside bulk Li_2O_2.

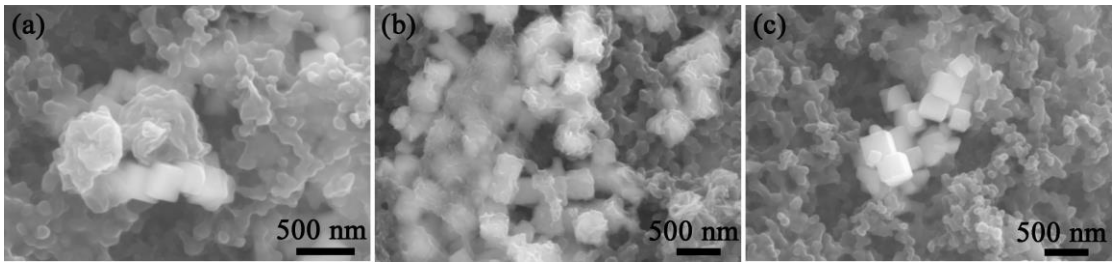

Figure S11. Ex-situ SEM images of three electrodes after fully recharged. (a) Co_3O_4. (b) S-Co_3O_4 and (c) P-Co_3O_4.

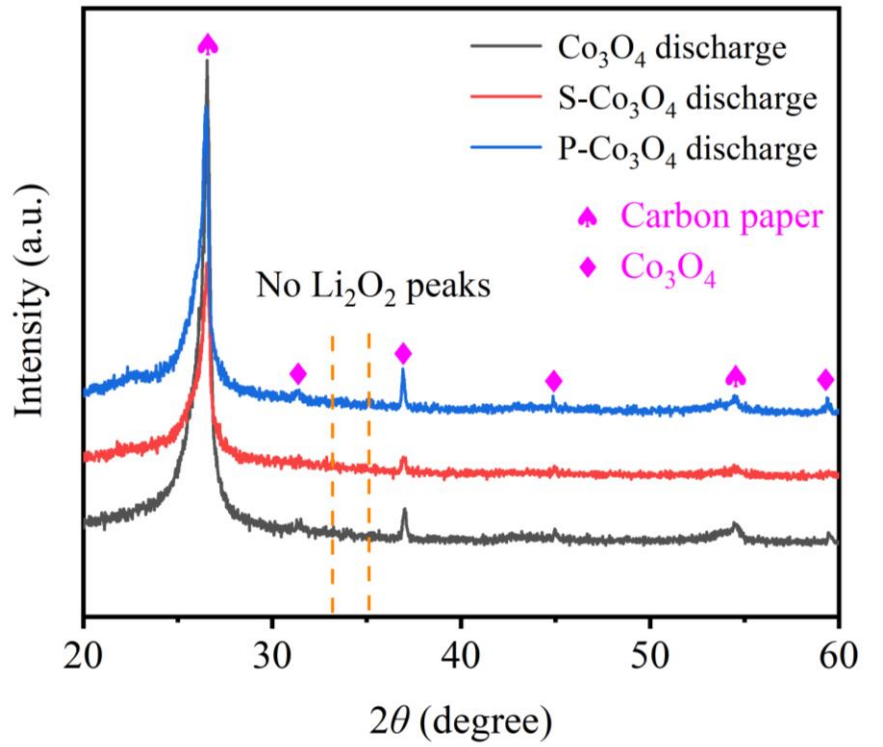

Figure S12. XRD patterns of three electrodes after first full recharge.

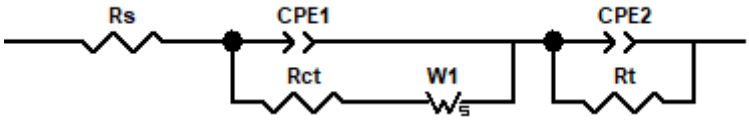

Figure S13. The corresponding equivalent circuit for EIS analysis.

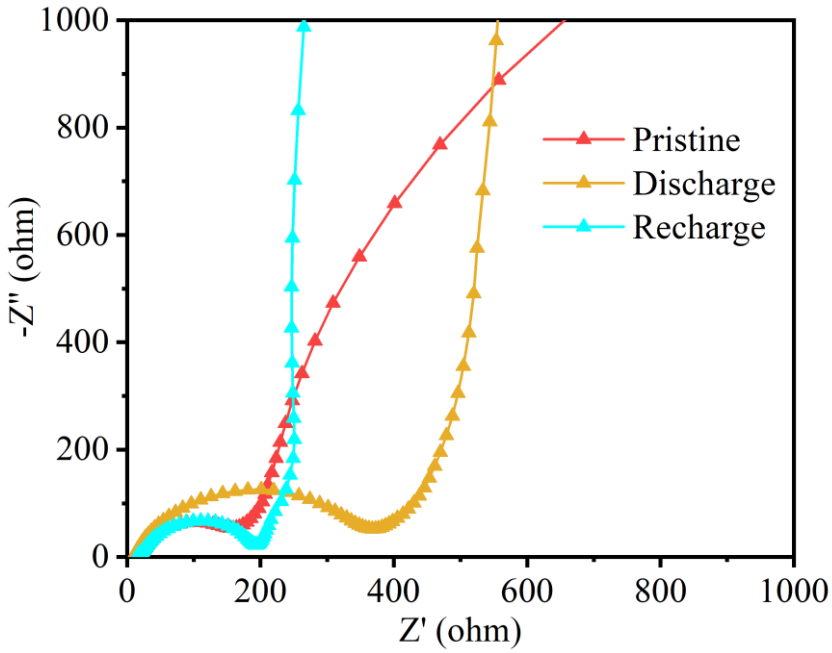

Figure S14. Nyquist plots of P-Co_3O_4 cathode at pristine and full discharge/recharge stage.

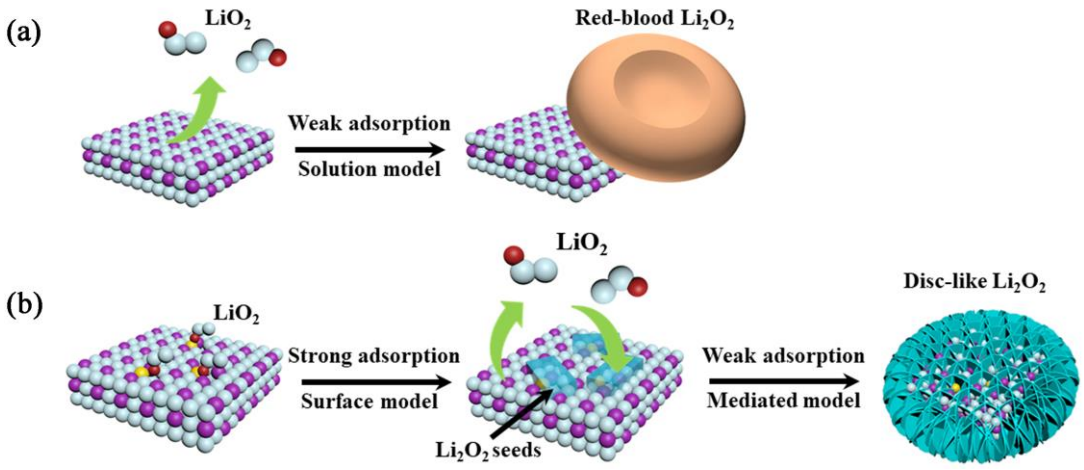

Figure S15. Schematic illustrations of the working mechanism for the (a) Co_3O_4 and (b) P-Co_3O_4 electrodes.

Table S1. Elemental contents of S-Co_3O_4 and P-Co_3O_4.

S or P (At%)	ICP-MS	EDS	XPS
S-Co_3O_4	1.21	0.54	4.72
P-Co_3O_4	1.16	0.64	3.95

The atomic percent contents measured by ICP-ES, EDS and XPS are quite different due to their intrinsic characteristics. The elemental contents given by ICP-ES reflect the true value of entire sample. However, XPS can only measure the depth of a few nanometers of sample surface. The testing depth EDS is larger than XPS but the value measured by EDS is not accurate. In view of heteroatom doping mainly on the surface, XPS results are closer to reality of doping than ICP-MS and EDS results.

Table S2. Comparison of electrochemical performance between some reported Co_3O_4-based cathodes for Li-O_2 batteries.

Catalysts	Over-potential (ORR/OER)	Discharge capacity (mAh g^{-1})	Cycle number/ cutoff capacity	Reference
Co_3O_4-(111)	**~1.5**	**2463**	**20/1000**	[5]
Co_3O_4 NS	**-**	**11882**	**80/500**	[6]
Co_3O_4 NFs/GNF	**1.26**	**10500**	**80/1000**	[7]
Co_3O_4-H	**~1.7**	**5220**	**110/500**	[8]
Co_3O_4-(112)	**~1.3**	**9144**	**50/500**	[9]
Co_3O_4@Co_3O_4/Ag	**~1.5**	**12000**	**80/1000**	[10]
P-Co_3O_4	**1.2**	**7690**	**90/1000**	**This**

References

1. Feng, J.; Zeng, H. Size-Controlled Growth of Co_3O_4 Nanocubes. Chemistry of Materials **2003**, *15*, 2829-2835.

2. Xiao, X.; Liu, X.; Zhao, H.; Chen, D.; Liu, F.; Xiang, J.; Hu, Z.; Li, Y. Facile shape control of Co_3O_4 and the effect of the crystal plane on electrochemical performance. *Advanced materials* **2012**, *24*, 5762-5766.

3. Jiang, Z.-L.; Xu, G.-L.; Yu, Z.; Zhou, T.-H.; Shi, W.-K.; Luo, C.-S.; Zhou, H.-J.; Chen, L.-B.; Sheng, W.-J.; Zhou, M. High rate and long cycle life in Li-O_2 batteries with highly efficient catalytic cathode configured with Co_3O_4 nanoflower. *Nano Energy* **2019**, *64*, 103896.

4. Lin, X.; Yuan, R.; Cai, S.; Jiang, Y.; Lei, J.; Liu, S.-G.; Wu, Q.-H.; Liao, H.-G.; Zheng, M.; Dong, Q. An Open-Structured Matrix as Oxygen Cathode with High Catalytic Activity and Large Li_2O_2 Accommodations for Lithium-Oxygen Batteries. *Advanced Energy Materials* **2018**, *8*, 1800089.

5. Gao, R.; Zhu, J.; Xiao, X.; Hu, Z.; Liu, J.; Liu, X. Facet-Dependent Electrocatalytic Performance of Co_3O_4 for Rechargeable Li-O_2 Battery. *The Journal of Physical Chemistry C* **2015**, *119*, 4516-4523.

6. Wu, F.; Zhang, X.; Zhao, T.; Chen, R.; Ye, Y.; Xie, M.; Li, L. Hierarchical mesoporous/macroporous Co_3O_4 ultrathin nanosheets as free-standing catalysts for rechargeable lithium-oxygen batteries. *Journal of Materials Chemistry A* **2015**, *3*, 17620-17626.

7. Ryu, W. H.; Yoon, T. H.; Song, S. H.; Jeon, S.; Park, Y. J.; Kim, I. D. Bifunctional composite catalysts using Co_3O_4 nanofibers immobilized on nonoxidized graphene nanoflakes for high-capacity and long-cycle Li-O_2 batteries. *Nano letters* **2013**, *13*, 4190-4197.

8. Zheng, Y.; Gao, R.; Zheng, L.; Sun, L.; Hu, Z.; Liu, X. Ultrathin Co_3O_4 Nanosheets with Edge-Enriched {111} Planes as Efficient Catalysts for Lithium-Oxygen Batteries. *ACS Catalysis* **2019**, *9*, 3773-3782.

9. He, M.; Zhang, P.; Xu, S.; Yan, X. Morphology Engineering of Co_3O_4 Nanoarrays as Free-Standing Catalysts for Lithium-Oxygen Batteries. *ACS applied materials & interfaces* **2016**, *8*, 23713-23720.

10. Gao, R.; Yang, Z.; Zheng, L.; Gu, L.; Liu, L.; Lee, Y.; Hu, Z.; Liu, X. Enhancing the Catalytic Activity of Co_3O_4 for Li-O_2 Batteries through the Synergy of Surface/Interface/Doping Engineering. *ACS Catalysis* **2018**, *8*, 1955-1963.